Oxidation kinetics of Cr-coated zirconium alloy: Effect of coating thickness and microstructure

E.B. Kashkarov[a,*], D.V. Sidelev[a], M.S. Syrtanov[a], C. Tang[b], M. Steinbrück[b]

[a] *National Research Tomsk Polytechnic University, School of Nuclear Science and Engineering, 634050 Tomsk, Russia*
[b] *Karlsruhe Institute of Technology, Institute for Applied Materials, 76344 Eggenstein-Leopoldshafen, Germany*

ABSTRACT

Cr coatings with the thickness of 4.5–9.0 μm and dense/columnar microstructure were deposited onto Zr alloy by cooled or hot target magnetron sputtering. Steam oxidation tests were performed under temperature ramp from 500 to 1200 °C and isothermal treatment at 900 1200 °C for 10 30 min. The measurements of mass gain showed different oxidation kinetics depending on microstructure and thickness of the as-deposited Cr coatings. The dense microstructure is favorable to prevent alloy oxidation as long as the Cr layer is intact. The higher activation energy of 202 kJ/mol is observed for the dense 4.5 μm-thick Cr coating while thicker columnar coatings have 177 183 kJ/mol. The time of transition from protective to non-protective behavior increases with coating thickness. It was shown that the 9 μm-thick Cr coating with columnar microstructure better protects the zirconium alloy from oxidation at 1200 °C for 10 min in comparison with thinner coatings. The fast inter-diffusion of Cr and Zr at coating/alloy interface significantly affects the oxidation kinetics of Cr-coated zirconium alloy at temperatures above 1100 °C and long oxidation time.

1. Introduction

Currently, significant efforts of academia and industry are directed to realize the short term strategy of Accident tolerant fuel (ATF) cladding for light water nuclear reactors [1 6]. The key approach is to create a protection coating to improve the resistance of zirconium claddings under normal operation (360 °C, 18.6 MPa, neutron irradiation), and emergency (in water vapor up to 1200 °C) situations. The most severe conditions for nuclear fuel claddings occur in the case of loss of coolant accident (LOCA) with the possibilities towards design extension conditions [7,8]. When the zirconium alloys (E110, E635, Zircaloys, M5, ZIRLO, etc.) interact with water vapor at high temperature (above 800 °C), it leads to Zr oxidation and embrittlement, and causes release of hydrogen and additional heat in view of exothermic oxidation reaction ($Zr + 2H_2O = ZrO_2 + H_2\uparrow$, $\Delta H = -584.5$ kJ/mol at 1200 °C).

Research performed by various groups worldwide, e.g. at CEA (France), CTU Prague (Czech Republic), JSC "VNIINM" (Russia), MIT (USA), etc. as well as our previous results [9 16] have shown that chromium is one of the most suitable candidates among the considered materials for protective coating. The Cr coatings have a reasonable cross section of neutron capture ($\sim$3.0 3.2 barn), low hydrogen permeability, high corrosion and radiation resistance, good adhesion and wear resistance, small difference in thermal expansion coefficients (($(6.2 10.2)\times10^{-6}$ 1/K) in comparison with zirconium (($(5.7 9.3)\times10^{-6}$ 1/K) from room temperature to 1000 °C. Among the coating techniques, magnetron sputtering systems have many favourable parameters [17,18]:

high coating purity;
wide range of operation characteristics (target power density of $10-50$ W/cm^2, bias potential up to $2-3$ kV, work pressure $\sim0.01-1$ Pa);
pulse parameters of power supplies (duty cycle $\sim0.05-1$, peak current and power density up to 3 5 A/cm^2 and $5-10$ kW/cm^2, etc.);
low thermal flux ($0.1-1$ W/cm^2) onto substrate during coating deposition.

These parameters can be used to regulate and control type (neutral or ion) and kinetic energy of deposited particles, crystal structure and microstructure of coating, adhesion, and their functional and mechanical properties. However, the cylindrical tube geometry of Zr alloy claddings with the length of $4-6$ m and less than 10 mm in diameter [19] may be challenging for the PVD coating procedure. Another major aspect is the high number of cladding tubes needed for nuclear reactors

---

[*] Corresponding author.
E-mail address: egor kashkarov@mail.ru (E.B. Kashkarov).

Table 1
Deposition parameters.

#	Q, W/cm^2	Magnetron	t, min	U_b, V	j_s, mA/cm^2	h, μm	T_{sub}, °C
Cr-4.5	31.4	multi-cathode	128	50	3.5	4.5 ± 0.1	330
Cr-6	39.5	with hot target	20		2.8	6.0 ± 0.2	380
Cr-9	39.5		30		2.8	9.0 ± 0.3	440

Note: Q – target power density; t – deposition time; U_b – bias potential; j_s – ion current density on a substrate; h – coating thickness; T_{sub} – substrate temperature.
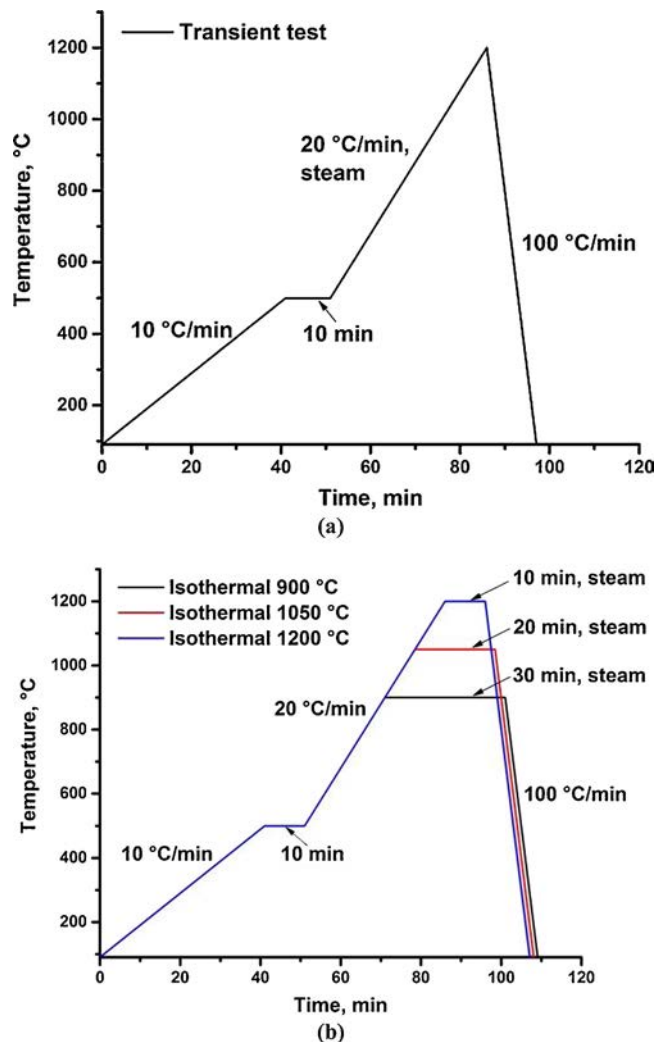

Fig. 1. Temperature profiles during the transient (a) and isothermal (b) tests.

every year (thousands of tubes and more), so the deposition technique should be highly productive and have high repeatability. Thus, new strategies of magnetron sputtering should be considered. Nowadays, the main approach is based on the classical magnetron sputtering, where several linear or cylindrical magnetrons (up to 4 – 6 m) or many short sized magnetrons (e.g. 400 mm in length) can be applied. The second way is to use the magnetron with hot target that has an ultra high deposition rate (50 nm/s and higher) [20 22]. However, it can sig nificantly influence the coating microstructure and functional proper ties. In the previous article [9], we have shown the role of the de position method on the resistance to high temperature oxidation in air atmosphere at 1100 °C during 20 min for Cr coated (1.8 4.5 μm) Zr 1Nb alloy. In the present paper, we will carefully consider the influence of deposition conditions on kinetics of zirconium oxidation at LOCA conditions, i.e. during high temperature oxidation in steam atmo sphere. Dense Cr coatings can be prepared by using of magnetron sputtering with high ion flux onto the substrate [23,24]. On the other hand, thicker Cr coatings with porous and columnar microstructure can be formed by hot target sputtering with high rates, when deposited particle flux is mainly composed of low energy sublimated particles [25,26].

The aim of the study is to determine the effect of thickness and coating microstructure on oxidation kinetics of Cr coated zirconium alloy in steam atmosphere. For this, the Cr coatings with different thickness and microstructure were deposited onto Zr alloy substrates by classical magnetron sputtering and with hot target. Then, the samples were oxidized in water vapor at 900, 1050 and 1200 °C with measuring their weight and post test examinations of crystal and microstructure.

2. Materials and methods

2.1. Coating deposition

The chromium coatings were deposited on E110 (Zr 1%Nb) alloy sheets (15 × 15 × 2 mm^3) and polished Si (110) substrates. The de tailed description of the installation has been reported in the previous work [27]. Chromium targets (∅ 90 mm and thickness of 8 mm; JSC Polema, Russia) with purity of 99.95 % were used. The 4.5 μm thick Cr coating with dense microstructure was obtained by the multi cathode magnetron sputtering system with "closed" [18,28,29] magnetic field and direct current (DC) power supply (Applied Electronics LLC, Russia). The high rate deposition of columnar Cr coatings (thickness of 6 and
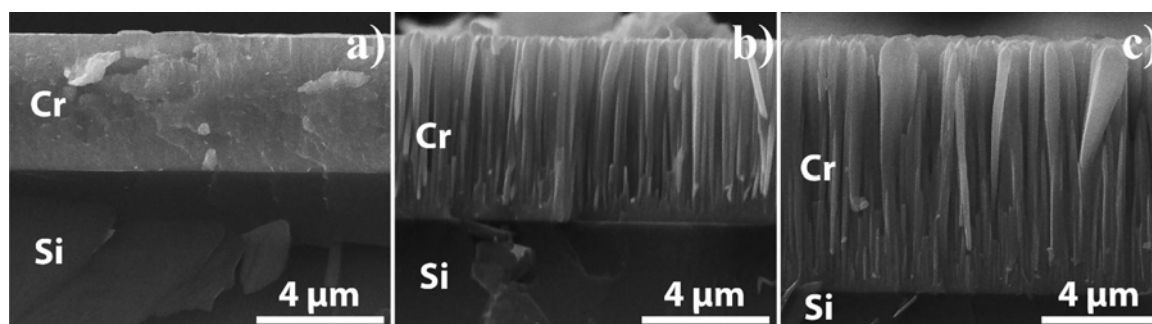

Fig. 2. The SEM images of the as-deposited Cr coatings: Cr-4.5 (a), Cr-6 (b) and Cr-9 (c).
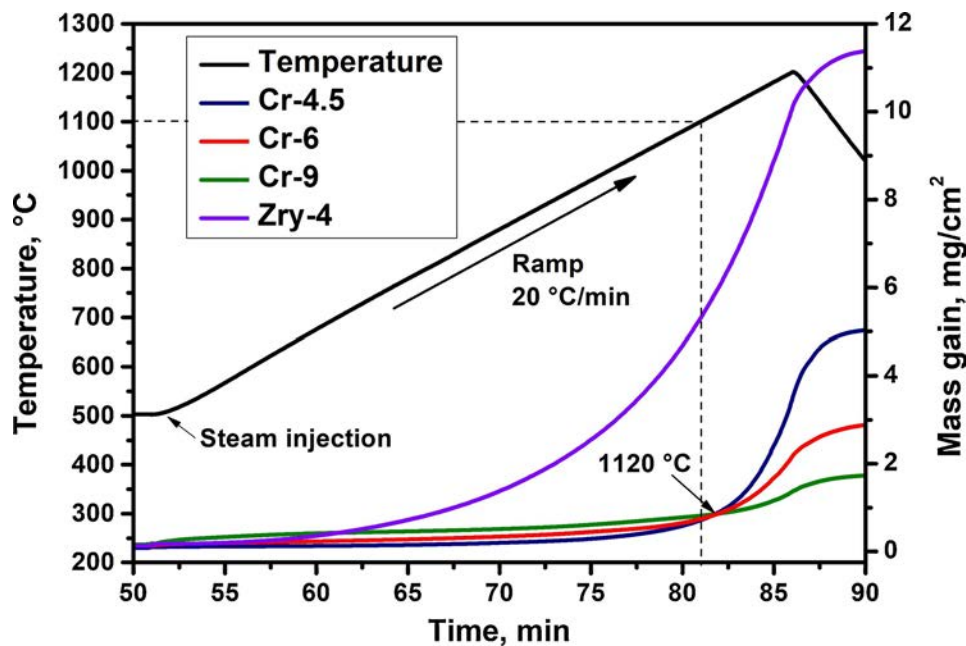
Fig. 3. Mass gain during the transient test of Cr-coated and uncoated zirconium alloys in steam flow at 500–1200 °C.

9 μm) was performed by hot target magnetron sputtering with DC power supply.

Prior to coating deposition, the E110 (Zr 1%Nb) alloy was cut onto small sheets (15 × 15 × 2 mm³) and holes with diameter of ⌀ 1 mm were drilled in these sheets for their holding during LOCA test. Then, to remove the surface oxides and other impurities, the samples were additionally pretreatment. Firstly, the samples were grinded and polished using SiC sandpapers (P600 → P4000), rinsed with 98 % alcohol for 2 min and dried by compressed air. The samples were fixed in stainless steel holders during coating deposition, thus, a small area of the Zr sheets (~8−9 mm²) remained uncoated. The distance from the Cr targets to the substrates during coating deposition was 100 mm. The base pressure in the vacuum chamber was 5·10⁻³ Pa. The operation pressure was 0.3 Pa (Ar). Before deposition, the substrates were etched by Ar⁺ ions at the following parameters: Ar pressure 0.15 Pa, acceleration voltage 2.5 kV, ion current 40 mA, treatment time 20 min. All substrates were planetary rotated during etching and deposition processes for uniform coating deposition. No preliminary or additional heating of the samples was carried out, the substrate temperature was measured by an infrared pyrometer Optris CTlaser 3MH1CF4 during coating deposition. Other parameters are shown in Table 1.

2.2. Oxidation tests

The oxidation tests were performed using a STA 449 F3 thermo gravimetric (TG) analyzing system (NETZSCH, Germany). Zircaloy 4 (Zry 4; Zr 1.5%Sn; 15 × 10 × 0.65 mm³) samples were used as the reference material. Firstly, a transient test was carried out to evaluate oxidation kinetics of the Cr coated E110 alloy and uncoated Zry 4 at high temperatures and to select duration of the isothermal tests. At the transient test, the samples were oxidized at temperature from 500 to 1200 °C in water steam with the heating rate of 20 °C/min (Fig. 1a). Isothermal oxidation tests were performed at 900, 1050 and 1200 °C for 30, 20 and 10 min, respectively (Fig. 1b). For each isothermal test, the temperature was stabilized for 1 min before injecting the steam flow (2 g/h). The samples were heated or cooled in protective Ar with a flow rate of 50 mL/min except the steam oxidation stage. The mass gain of the samples during oxidation tests was in situ measured in the TG system. Additionally, the weight of the samples was also measured before and after oxidation tests using an analytical balance (AE 240,

Mettler). In the TG tests, the thermocouple was not in direct contact to the sample. Therefore, the exothermic oxidation reaction between zirconium and steam can cause overheating of the reference Zry 4 sample and results in accelerated oxidation kinetics at the initial stage. It should be less important for Cr coated samples with lower initial oxidation rates.

The samples with Cr films (Cr 4.5, Cr 6 and Cr 9) had the uncoated corner, so their mass gain and oxidation kinetics some increased due to rapid oxidation of E110 alloy without protective coating. According to the experimental data, the mass gain of uncoated part (~8−9 mm²) was equal to ~0.41, 1.41 and 2.77 mg at 900, 1050 and 1200 °C for the given samples and oxidation conditions. This should be taken into account for considering and comparing with other published results.

2.3. Post test examinations

The phase composition of the as deposited and oxidized samples was analysed by X ray diffraction (XRD) using Shimadzu XRD 7000S diffractometer equipped with 1280 channel high speed detector (OneSight, Japan). The XRD analysis was performed in Bragg Brentano geometry using Cu Kα radiation (1.5410 Å wavelength) at 40 kV and 30 mA. The diffraction data were analysed by means of the Sleve + program. The coating thickness, microstructure and elemental composition of the samples were investigated by a scanning electron microscope (SEM) Vega 3 (Tescan, Czech Republic) equipped with energy dispersive X ray spectroscopy (EDX) attachment. The microstructure of the oxidized samples was also analysed by optical microscopy using AXIOVERT 200MAT (Zeiss, Göttingen, Germany). The elemental distribution of the samples over depth was investigated by glow discharge optical emission spectroscopy (GDOES) using GD Profiler 2 (HORIBA Scientific, Japan). All post test examinations were performed only for central part of the samples.

3. Results

3.1. The as deposited Cr coatings

Fig. 2 shows the thickness and microstructure of the as deposited Cr coatings on Si substrates. It can be seen that the deposition method strongly affects the coating growth. The dense Cr coating with an
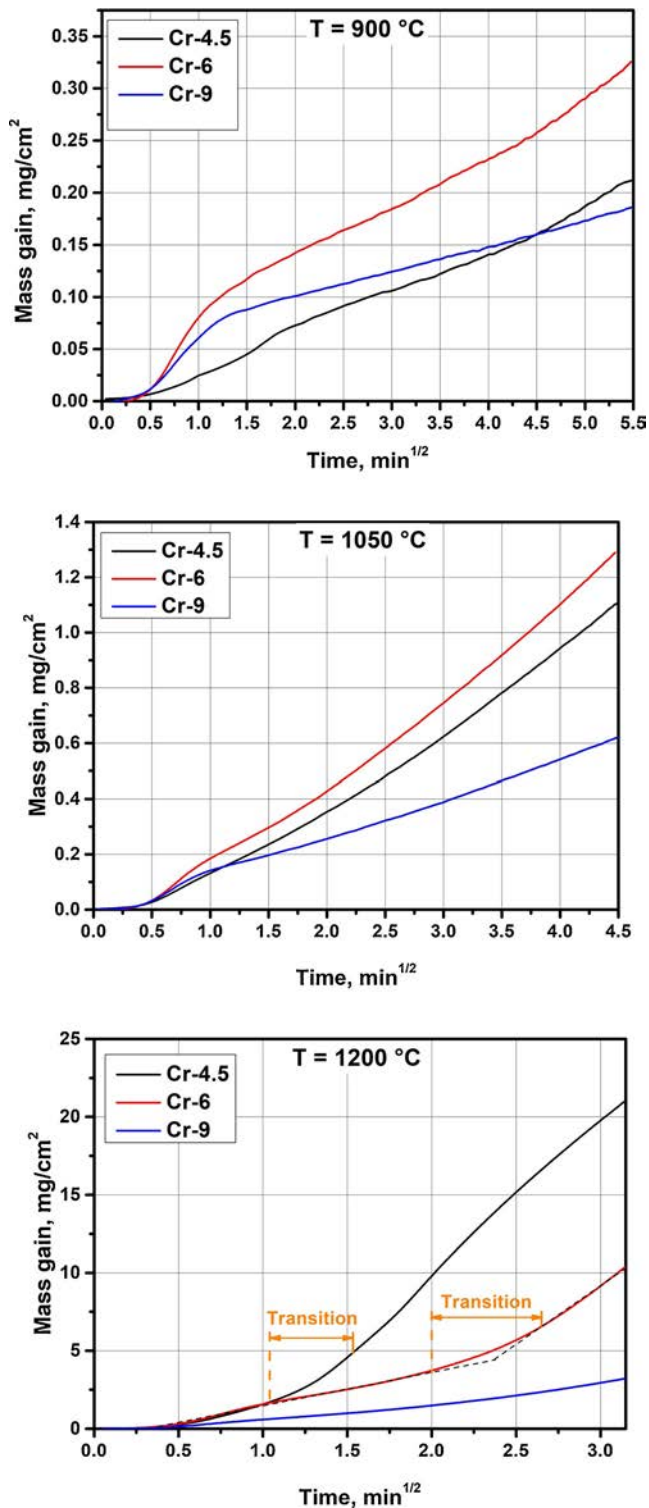
Fig. 4. The mass gain during oxidation of Cr-coated zirconium alloy in steam flow at 900, 1050 and 1200 °C.

absolute deposition rate of 6 nm/s (i.e. for the unmoved substrate) was deposited by multi cathode magnetron sputtering (Fig. 2a). In this case, energy flux per one deposited atom (31.2 eV/atom) and ion current density to the substrate (3.5 mA/cm²) are high enough to cause in tensive surface diffusion and coating densification [9,23]. On the other hand, Cr coatings were obtained at high deposition rates ($\sim$50 nm/s) using hot target sputtering technique (Fig. 2b and c). In that case the majority particles were sublimated from hot target and had low

($\sim$0.1 eV) kinetic energy [25] in the deposition flux. So, the energy flux per one deposited atom is equal to $\sim$3.2 eV/atom. Thus, porous Cr coatings are formed with V shaped columnar grains perpendicular to the substrate surface (zone T according to the structural zone model (SZM) [30,31]). Fig. 2b,c show that the column width increases with coating thickness (6 $\rightarrow$ 9 µm) due to higher adatom mobility with substrate heating from 380 to 440 °C at the same deposition rate (see Table 1). Earlier [9], we have shown the influence of deposition rate and energy flux on microstructure for 1.8 4.5 µm thick Cr coatings. According to XRD data, the as deposited Cr coatings have a body cen tered cubic (bcc) crystalline phase with a strong (110) orientation.

3.2. Transient test at 500 − 1200 °C

Fig. 3 shows the TG results of mass gain measured for the Cr coated E110 alloy and uncoated reference sample during heating in the steam flow at 500 − 1200 °C. The obtained curves demonstrate that the in tensive oxidation of the uncoated Zr alloy occurs at $\sim$620 °C and the mass gain of 11.38 mg/cm² was reached at 1200 °C. The chromium coatings improve the oxidation resistance of zirconium alloy in steam during temperature ramp. The transition temperature to accelerated oxidation kinetics is increased up to 1050 − 1100 °C. The sample with the Cr 4.5 coating reveals the lowest rate of mass gain at the initial stage (temperature lower than 1100 − 1120 °C). Then, this sample de monstrates the pronounced rise of mass gain up to 5.03 mg/cm² at 1200 °C. The samples with Cr 6 and Cr 9 coatings have similar beha vior, but the mass gain is slightly higher at temperatures below 1100 °C. Above 1100 °C, the oxidation kinetics are lower for thicker coatings: the total mass gain was 1.73 mg/cm² for 9 µm thick Cr coating and 2.88 mg/cm² for 6 µm thick Cr coating.

3.3. Isothermal tests at 900 − 1200 °C

Fig. 4 shows the TG results during steam oxidation at 900, 1050 and 1200 °C for the Cr coated samples. For the temperature range of 900 − 1050 °C, the columnar coatings demonstrate different oxidation kinetics at the initial stage and continuous oxidation. It can be seen that columnar Cr films intensively oxidized at the initial stage from the moment of steam injecting up to 1 − 1.2 min (at temperatures up to 1050 °C). As a result, a protective oxide layer is formed and the oxi dation kinetics slows down significantly. The oxidation behavior of the dense Cr coating is the same, but the oxidation rate at the initial stage is not much different from further oxidation, i.e. there is no sharp cap turing of oxygen (Fig. 4a and b). Typical parabolic kinetics is observed for Cr coated samples at 900 and 1050 °C during the stage of continuous oxidation, while at 1200 °C the TG curves have a characteristic transi tion from protective to non protective scale (Fig. 4c). This transition is accompanied by an acceleration of oxidation kinetics and defined as the time of transition period marked in Fig. 4c for Cr 4.5 and Cr 6 coatings. For better understanding and comparison of the results, we summarized the mass gain data and the corrosion rates in Table 2. It should be noted that the high mass gains for the reference Zry 4 alloy can be caused by their overheating due to a strong exothermic reaction between zirco nium and steam. Thus, the obtained mass gains exceed approx. two times the values predicted by Cathcart Pawel model and other experi mental data for the steam oxidation at 1200 °C [32,33].

The corrosion rates of the experimental samples were obtained by fitting the TG curves using the following equation:

$$\Delta m = K \cdot t^n \tag{1}$$

where Δm mass gain (mg/cm²); K rate constant; t time; n rate exponent (fixed to 0.5 for parabolic kinetics).

It is shown that the Cr 4.5 sample has the lowest mass gain (0.31 mg/cm²) compared to the Zr alloy with columnar coatings at 900 °C. For higher oxidation temperature (1050 °C), the rate constant of the Cr 4.5 sample is between the rates for columnar coatings (6 and

T, °C	#	S, cm^2	Δm (TGA), mg/cm^2	Δm (an. bal.), mg/cm^2	Rate constant, mg/cm^2·min$^{1/2}$
900	Cr-4.5 (dense, 4.5 μm)	5.43	0.31	0.33	0.04
	Cr-6 (columnar, 6.0 μm)	5.62	0.57	0.52	0.05
	Cr-9 (columnar, 9.0 μm)	5.30	0.49	0.45	0.02
	Zry-4 (uncoated)	3.20	4.70	4.75	1.12
1050	Cr-4.5 (dense, 4.5 μm)	5.09	1.40	1.38	0.29
	Cr-6 (columnar, 6.0 μm)	5.68	1.64	1.59	0.33
	Cr-9 (columnar, 9.0 μm)	5.43	1.03	1.00	0.14
	Zry-4 (uncoated)	3.40	16.44	16.50	3.95
1200	Cr-4.5 (dense, 4.5 μm)	5.58	22.90	22.87	2.70 / 10.20*
	Cr-6 (columnar, 6.0 μm)	5.67	12.61	12.59	2.09 / 7.80*
	Cr-9 (columnar, 9.0 μm)	5.35	4.13	4.09	1.12
	Zry-4 (uncoated)	3.40	32.50	32.59	–

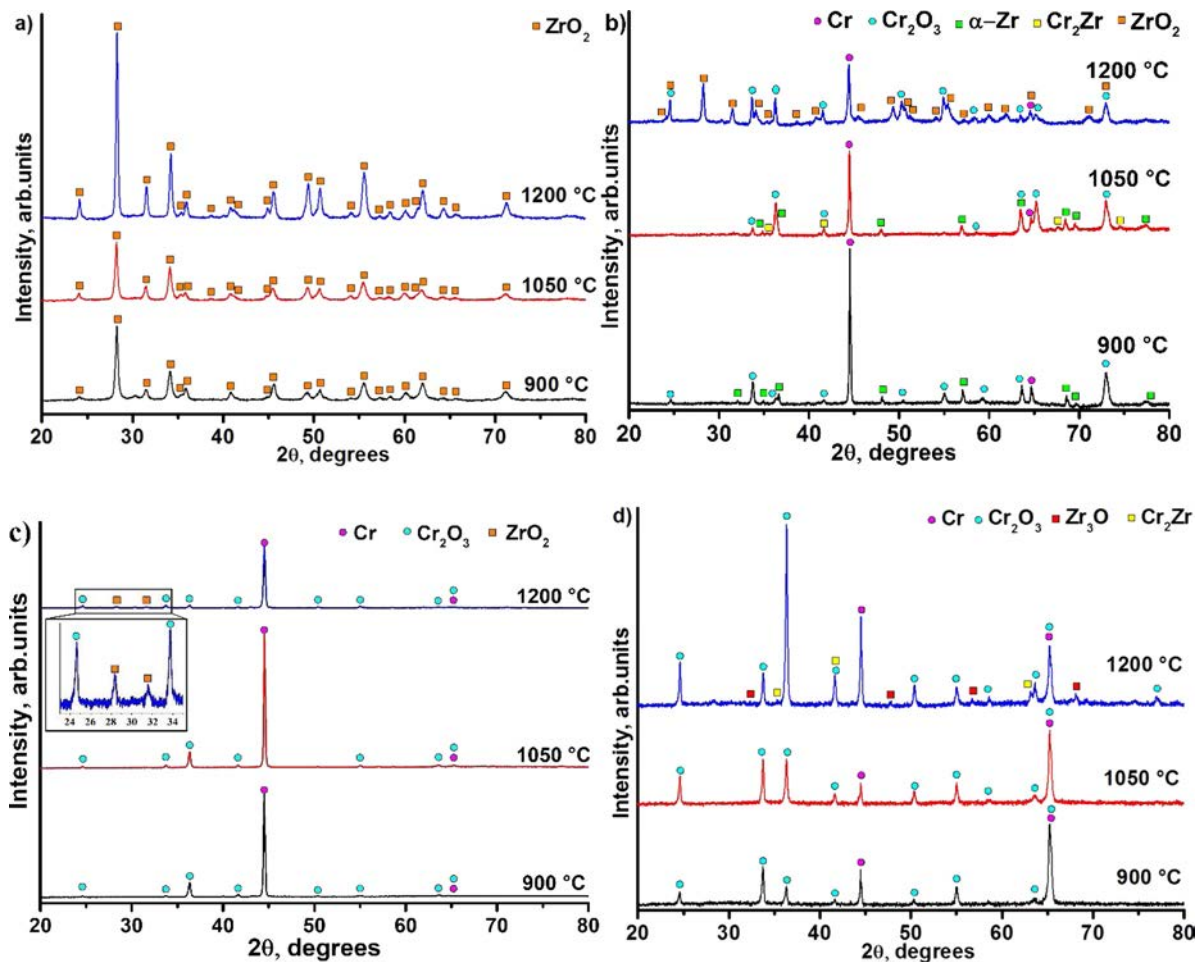* Rate constant after transition from protective to non-protective scale.

Fig. 5. Diffraction patterns of the samples after the isothermal tests: a – uncoated Zry-4; b – Cr-4.5; c – Cr-6; d – Cr-9.

9 μm thick). Nevertheless, at 1200 °C the Cr 4.5 sample has the biggest mass gain for 10 min oxidation (22.90 mg/cm^2), whereas the Zr alloy with thicker Cr coatings have lower mass gain values of 12.61 mg/cm^2 for Cr 6 and 4.13 mg/cm^2 for Cr 9 samples.

The XRD patterns and phase composition of the Cr coated and un coated Zr alloys after isothermal oxidation at 900 − 1200 °C are shown in Fig. 5. Only ZrO$_2$ (monoclinic) phase is formed on the surface of uncoated Zry 4 alloy at the investigated temperatures. For the Cr 4.5 sample, the Cr (bcc) phase is decreased for 900 →1200 °C, the forma tion of Cr$_2$Zr (at 1050 °C) and ZrO$_2$ (at 1200 °C) phases is observed. The phase composition of Zr alloys coated by columnar Cr coatings after

oxidation at 900 and 1050 °C is represented by Cr$_2$O$_3$ and Cr phases. The monoclinic ZrO$_2$ phase was detected for the Cr 6 oxidized at 1200 °C, whereas, the sample with thicker Cr (9 μm) coating has only inter diffusion Cr$_2$Zr and oxygen stabilized α Zr(O) phases.

Fig. 6 presents the cross section images of the samples after oxida tion at 1200 °C for 10 min. The microstructure of the Zry 4 alloy is re presented by the outer ZrO$_2$ layer (more than 190 − 250 μm) at both sides and the internal oxygen stabilized α Zr(O) phase (Fig. 6a).

According to the optical microscopy images (Fig. 6b d) and GDOES data (Fig. 7), the Cr coated Zr alloy after oxidation has different structure:
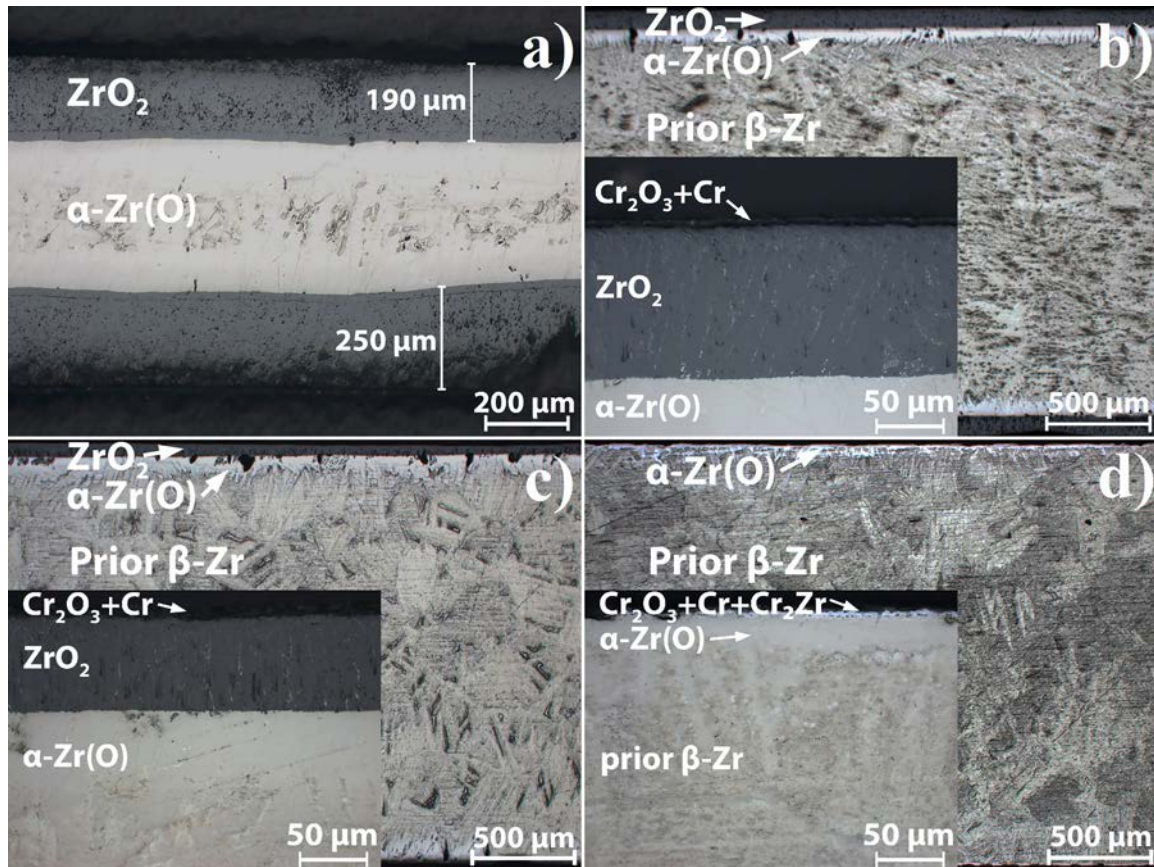
Fig. 6. Optical images of the cross-sections after steam oxidation at 1200 °C for 10 min: uncoated Zry-4 (a), Cr-4.5 (b), Cr-6 (c) and Cr-9 (d).

the protective Cr_2O_3 layer with residual Cr (or Cr + ZrO_2);
the Cr_2Zr inter diffusion layer (only for Cr 9);
the ZrO_2 layer with the thickness of 85 110 and 50 − 70 μm for Cr 4.5 and Cr 6;
oxygen stabilized α Zr(O) phase with non uniform thickness;
the internal prior β Zr phase.

The profiles reveal oxidation of Cr coated alloy and noticeable inter diffusion of Cr and Zr at the coating/alloy interface. Depending on the coating type, the formation of different multilayer structures was found. So, the Cr 4.5 and Cr 6 samples have similar elemental distribution over the sputtering depth of 20 μm: outer chromia (1.9 2.4 μm) → residual Cr with ZrO_2 grains (up to ~6 μm) → thick ZrO_2 layer (Fig. 7a and b). Most likely the growth of zirconium oxide phase in the residual Cr is caused by the oxidation of earlier formed Cr_2Zr phase in high inward oxygen flux (see Eq. (2) in [10]).

GDOES and SEM observations show that Cr 9 is fully protective at 1200 °C for 10 min, no ZrO_2 layers are found at both sides of the sample (Fig. 7c). There is the protective Cr_2O_3 layer (~3.5 μm) at the surface, residual Cr (up to 5.5 μm), non uniform inter diffusion Cr Zr layer, α Zr (O) layer with the thickness of ~15 − 30 μm. Under these oxidation conditions, the Cr_2Zr layer has 1.9 2.7 μm thickness that well correlates with the recent studies [9,12,34]. The importance of coating thickness and microstructure at high temperatures is also evidenced by several possible processes: Cr volatilization [10,16] with formation of gaseous species and delamination/cracking of the protective Cr_2O_3 layer at the oxide/metal interface. Moreover, the Cr_2O_3 layer can be reduced by zirconium due to higher thermodynamic stability of zirconia compared to chromia. In this process Zr atoms can transfer electrons to Cr_2O_3 reducing Cr ions to neutral atoms and the free oxygen ions can diffuse and react with Zr^{4+} to form ZrO_2 phase [10,35]. These mechanisms are also supported by changes of phase composition with temperature rise

by XRD and SEM in this study.

4. Discussion

The multi cathode magnetron with "closed" magnetic field config uration has low deposition rate (~6 nm/s) and high energy flux to substrate, so it can produce the dense Cr coatings. Contrary, the mag netron with hot target can be used for high rate Cr deposition (~50 nm/s), but the deposited coatings have porous and columnar microstructure due to low energy flux to substrate. Both constructions of magnetron sputtering systems were used for deposition of the Cr (4.5 9.0 μm thick) coatings with dense or columnar microstructure onto E110 alloy. The presented results show that microstructure and coating thickness significantly affect the oxidation kinetics of Cr coated zirconium alloy in water steam in the temperature range 900 − 1200 °C. To evaluate this phenomenon, Arrhenius plots were constructed based on the data of linear approximation of continuous oxidation process at 900 and 1050 °C (Fig. 8). For 1200 °C, the linear approximation of the experimental data was carried out before the transition period, which characterizes the oxidation process of Cr coating. The linear curves of ln (R_t) vs. $(1/T)$ for the Cr coated Zr alloy are fitted according to the Ar rhenius equation:

$$K_t = A \cdot \exp(E_a/R \cdot T), \tag{1}$$

where A the pre exponential constant; E_a the activation energy for oxidation process; R the gas constant (8.31 J/mol·K); T the tem perature (K).

The Zr alloy coated by the dense Cr film (Cr 4.5) has significantly higher activation energy (202 kJ/mol) compared to the samples with the columnar (177 − 183 kJ/mol) coatings, which confirms its better protective properties during steam oxidation. However, higher value of A (3.4·10^7) for the Cr 4.5 indicates the decrease of corrosion resistance
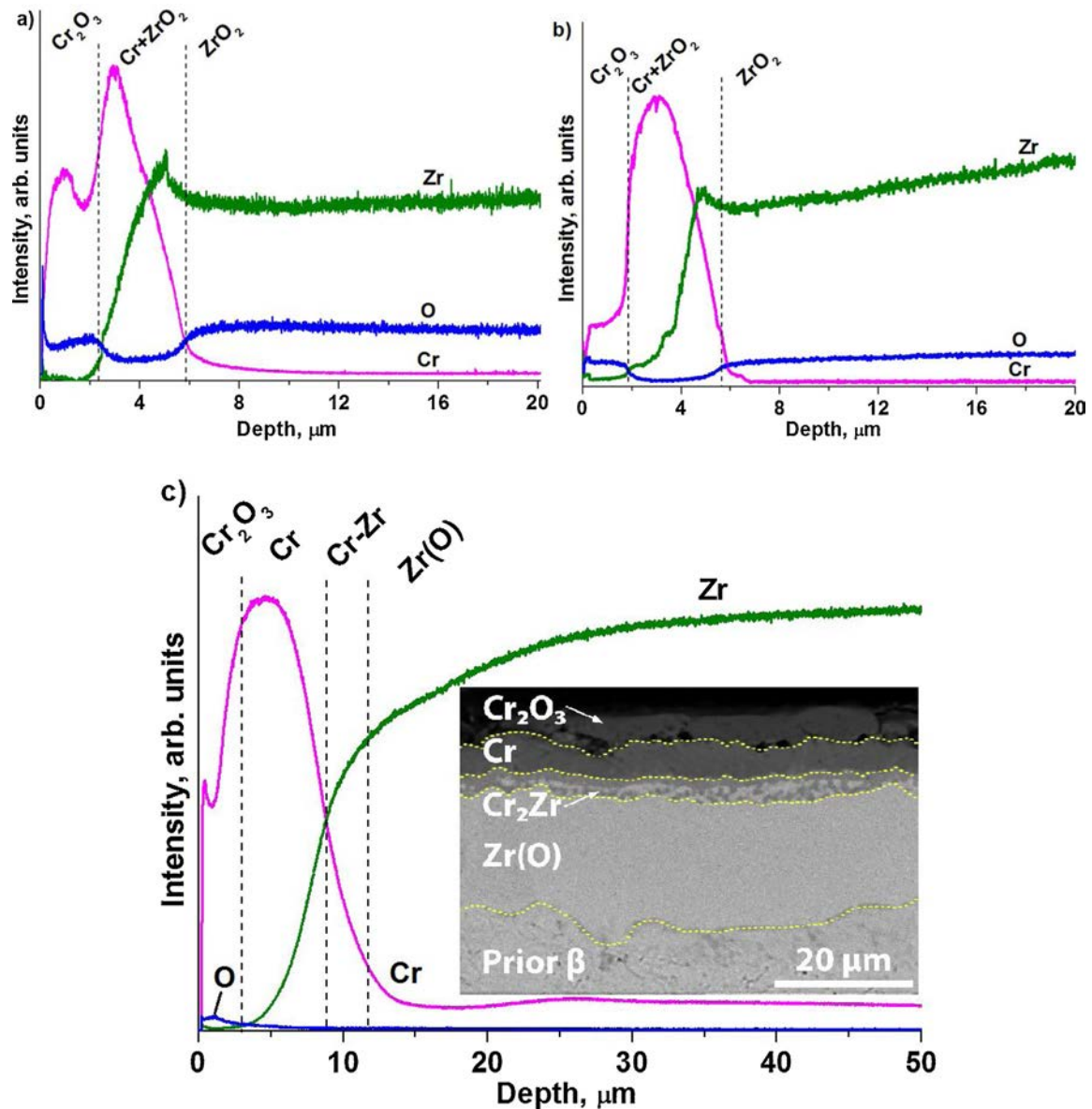
Fig. 7. GDOES depth distribution profiles of elements in the Cr-coated Zr samples after oxidation at 1200 °C for 10 min: Cr-4.5 (a), Cr-6 (b) and Cr-9 (c). Inset: cross-section SEM image of the oxidized Cr-9 sample.

concerning to the samples with thicker coatings (Cr 6 $4.0 \cdot 10^6$; Cr 9 $2.9 \cdot 10^6$) at higher oxidation temperature. The obtained activation energy for the dense Cr coating is comparable or higher than the values reported for Cr coated zirconium alloy [10] and pure bulk chromium in air or oxygen [36 38], but slightly lower than for CrN coated Zr [39]. Even if the order of magnitude seems to be consistent with some literature data, one should be cautious about the "physical meaning" of the apparent activation energy derived from the overall weight gain evolutions due to potential effects of some experimental bias (temperature overshoot and contribution of unprotected sample areas).

At low temperatures, the oxidation of Cr coatings is only expected: no ZrO_2 phase in the alloy can be detected after oxidation at 900 °C (30 min) and 1050 °C (20 min). Under these conditions, the mass gain is extremely low ($0.31 - 1.64 \, mg/cm^2$), whereas it should be $\geq 4 - 7 \, mg/cm^2$ [9 11,27] to form ZrO_2 layer beneath the $1 - 10 \, \mu m$ thick Cr coatings. Thus, the low mass gain of the samples is caused by the formation of the protective Cr_2O_3 layer on coating surface that has a strong oxidation resistance in steam up to 1100 °C [40]. Nevertheless, the different oxidation kinetics of the Cr coatings is observed depending on their microstructure. The initial stage of oxidation for columnar

coatings is accompanied by a rapid weight gain, while for the dense coating it is changed gradually (Figs. 3 and 4). This behavior is attributed to grain boundary oxygen diffusion until the external protective chromia layer is formed. Thus, the growth of the oxide layer in the dense Cr coating occurs with lower rates. It results the lowest oxidation kinetics of the dense Cr 4.5 compared to columnar ones. Next, the continuous oxidation of the residual Cr can be accompanied by Cr_2O_3 growth and formation of Cr_2Zr interlayer beneath the residual Cr. For columnar coatings, α Zr(O) can also be formed due to oxygen diffusion along grain boundaries. Thus, at this temperature range, the dense Cr coating has higher oxidation resistance even with a thinner Cr_2O_3 layer (900 °C $0.31 \, mg/cm^2$). Oppositely, the columnar Cr coatings can be oxidized for higher depth in view of their porous microstructure (0.49 and $0.57 \, mg/cm^2$).

The oxidation of Cr coated Zr alloy is accelerated with temperature rise. This is clearly seen from the balancing of mass gains at the transient tests at 1100 °C ($\sim 0.86 \, mg/cm^2$) and increase of mass gain for isothermal test at 1050 °C. This means the rise of oxygen diffusion through the protective layer to a residual Cr and, deeper, in the Zr alloy. There are several processes that should be mentioned:
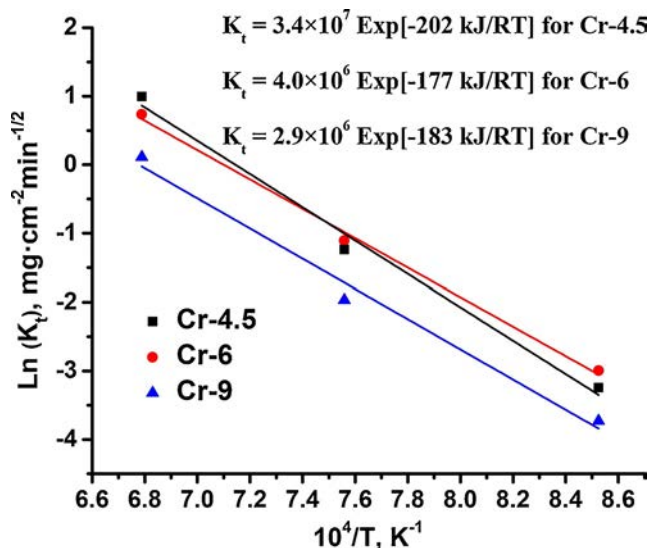
$$K_t = 3.4 \times 10^7 \, Exp[-202 \, kJ/RT] \text{ for Cr-4.5}$$
$$K_t = 4.0 \times 10^6 \, Exp[-177 \, kJ/RT] \text{ for Cr-6}$$
$$K_t = 2.9 \times 10^6 \, Exp[-183 \, kJ/RT] \text{ for Cr-9}$$

Fig. 8. The Arrhenius plots for Cr-coated Zr alloy in a steam.

the inter diffusion of Cr and Zr due to high diffusion coefficient of Cr into β Zr phase [41] and growth of Cr_2Zr phase that is found by XRD for the sample with thinner Cr coating even for 1050 °C;

the formation of Kirkendall cavities at the Cr_2O_3/Cr and Cr Zr in terfaces [10];

shorter diffusion path of O to the Zr alloy through thinner protective coating.

The inter diffusion of Cr and Zr becomes more significant during oxidation at 1200 °C, with higher diffusion coefficients for Cr into Zr. The influence of coating thickness and Cr Zr interlayer on oxidation kinetics of Cr coated Zr alloy can be demonstrated by the different evolution of mass gains at 1200 °C (Fig. 4).

The Cr 9 sample remains fully protective during 10 min exposure at 1200 °C ($4.13 \, mg/cm^2$), no ZrO_2 phase is found beneath the Cr Zr in terlayer. The transition region with the accelerated oxidation is ob served for the Cr 6 sample. This corresponds to degradation of pro tective properties of 6 µm thick Cr coating, i.e. transition from protective to non protective scale. Brachet et al. [10] showed that the new oxidation mechanism of Cr coated Zr alloy can be activated at this stage. The latter is associated with outward diffusion of zirconium re sulting nucleation of zirconia stringers at the Cr grain boundaries, which promotes the diffusion of oxygen anions through the coating (zirconia networks).

The relatively thin coated Cr 4.5 sample shows poor protective properties under steam oxidation at 1200 °C ($22.9 \, mg/cm^2$). Due to lower coating thickness (4.5 µm) and fast inter diffusion of Cr and Zr at high temperatures, the oxygen diffusion path is strongly decreased and the coating can be protective only for a short oxidation period (~ 2 min, see Fig. 4c). It results in the formation of thick ($\sim 70 - 110$ µm) zirconia layer beneath the oxidized coating (Fig. 6b). Therefore, the overall oxidation kinetics of the Cr 4.5 sample is mainly defined by Zr substrate oxidation (non protective oxide scale).

Therefore, based on the described results, we suggest several aspects in oxidation of the Cr coated Zr alloy. As long as the Cr coating is still protective, the microstructure of the Cr layer strongly affects the oxi dation kinetics of the Cr coated Zr alloy. The time until transition from protective to non protective behavior at high temperatures is mainly determined by the thickness of Cr layer. However, dense microstructure of protective coatings is desirable to prevent the formation of brittle α Zr(O) layer due to oxygen diffusion through the columnar grain boundaries. For higher temperatures ($1100 - 1200$ °C) or longer oxi dation time, fast inter diffusion of Cr and Zr with formation of Cr_2Zr

phase becomes more important in oxidation kinetics.

5. Conclusions

For the oxidation temperature range of $900 - 1200$ °C, the Cr coat ings deposited by magnetron sputtering onto zirconium alloy can be a fully protective in steam environment. Their oxidation kinetics for $10 - 30$ min was studied as a function of coating microstructure and thickness. The main conclusions are the following.

1 As long as the Cr coating is intact/protective, which is given up to 1100 °C for reasonable times relevant for LOCA scenarios, the mi crostructure of the Cr coatings is a key characteristic in accident conditions. The results show that a dense 4.5 µm thick Cr coating with higher activation energy (202 kJ/mol) provides better oxida tion resistance up to 1100 °C compared to thicker (6 and 9 µm) co lumnar coatings ($177 - 183$ kJ/mol).

2 An accelerated oxidation kinetics of Cr coated Zr alloy is observed after transition from protective to non protective behavior. The duration of protective period is mainly dependent on the coating thickness. Thicker protective coatings have longer diffusion path of O to the Zr alloy in the conditions of Cr consumption by Cr Zr inter diffusion. The 9 µm thick columnar Cr coating fully protects the E110 alloy from oxidation at 1200 °C for 10 min, while the 4.5 6.0 µm thick Cr coatings does not at the same oxidation condi tions.

3 The fast inter diffusion of Cr and Zr with Cr_2Zr formation at the coating/alloy interface at higher temperatures (> 1100 °C) and for longer oxidation time can significantly decrease the protective properties of the Cr coatings. These aspects cause poor efficiency of Cr coatings with low thickness for Zr fuel claddings at LOCA con ditions.

Declaration of Competing Interest

The authors declare that there are no conflicts of interest.

References

[1] C. Tang, M. Stueber, H.J. Seifert, M. Steinbrueck, Protective coatings on zirconium-based alloys as accident-tolerant fuel (ATF) claddings, Corros. Rev. 35 (2017) 141–165, https://doi.org/10.1515/corrrev-2017-0010.

[2] Z. Duan, H. Yang, Y. Satoh, K. Murakami, S. Kano, Z. Zhao, J. Shen, H. Abe, Current status of materials development of nuclear fuel cladding tubes for light water reactors, Nucl. Energy Des. 316 (2017) 131–150, https://doi.org/10.1016/j.nucengdes.2017.02.031.

[3] M. Wagih, B. Spencer, J. Hales, K. Shirvan, Fuel performance of chromium-coated zirconium alloy and silicon carbide accident tolerant fuel claddings, Ann. Nucl. Energy 120 (2018) 304–318, https://doi.org/10.1016/j.anucene.2018.06.001.

[4] J.C. Brachet, M.L. Saux, M.L. Flem, S. Urvoy, E. Rouesne, T. Guilbert, et al., Ongoing studies at CEA on chromium coated zirconium based nuclear fuel claddings for enhanced accident tolerant LWRs fuel, Proc. 2015 LWR Fuel Perform/TopFuel (2015) 31–38.

[5] K.A. Terrani, Accident tolerant fuel cladding development: promise, status, and challenges, J. Nucl. Mater. 501 (2018) 13–30, https://doi.org/10.1016/j.jnucmat.2017.12.043.

[6] M. Huang, Y. Li, G. Ran, Z. Yang, P. Wang, Cr-coated Zr-4 alloy prepared by electroplating and its in situ He$^+$ irradiation behavior, J. Nucl. Mater. 538 (2020) 152240, , https://doi.org/10.1016/j.jnucmat.2020.152240.

[7] J. Bischoff, C. Delafoy, C. Vauglin, P. Barberis, C. Roubeyrie, D. Perche, et al., AREVA NP's enhanced accident-tolerant fuel developments: focus on Cr-coated M5 cladding, Nucl. Eng. Technol. 50 (2018) 223–228, https://doi.org/10.1016/j.net.2017.12.004.

[8] J.C. Brachet, T. Guilbert, M. Lesaux, J. Rousselot, G. Nony, et al., Behavior of Cr-Coated M5 Claddings During and After High Temperature Steam Oxidation From 800 C up to 1500 C. Topfuel 2018, Sep 2018, Prague, Czech Republic, ffcea-02328975 (2018).

[9] E.B. Kashkarov, D.V. Sidelev, M. Rombaeva, M.S. Syrtanov, G.A. Bleykher, Chromium coatings deposited by cooled and hot target magnetron sputtering for accident tolerant nuclear fuel claddings, Surf. Coat. Technol. 389 (2020) 125618, , https://doi.org/10.1016/j.surfcoat.2020.125618.

[10] J.C. Brachet, E. Rouesne, J. Ribis, T. Guilbert, S. Urvoy, G. Nony, et al., High temperature steam oxidation of chromium-coated zirconium-based alloys: kinetics and process, Corros. Sci. 167 (2020) 108537, , https://doi.org/10.1016/j.corsci.2020.108537.

[11] J.C. Brachet, I. Idarraga-Trujillo, M. Le Flem, M. Le Saux, V. Vandenberghe, et al., Early studies on Cr-coated Zircaloy-4 as enhanced accident tolerant nuclear fuel claddings for light water reactors, J. Nucl. Mater. 517 (2019) 268–285, https://doi.org/10.1016/j.jnucmat.2019.02.018.

[12] J. Krejcí, J. Kabátová, F. Manoch, J. Kočí, L. Cvrček, J. Málek, et al., Development and testing of multicomponent fuel cladding with enhanced accidental performance, Nucl. Eng. Technol. 52 (2020) 597–609, https://doi.org/10.1016/j.net.2019.08.015.

[13] W. Xiao, H. Chen, X. Liu, D. Tang, H. Deng, S. Zou, Y. Ren, X. Zhou, M. Lei, Thermal shock resistance of TiN-, Cr-, and TiN/Cr-coated zirconium alloy, J. Nucl. Mater. 526 (2019) 151777, , https://doi.org/10.1016/j.jnucmat.2019.151777.

[14] M. Sevecek, A. Gurgen, A. Seshadri, Y. Che, M. Wagih, B. Phillips, V. Champagne, K. Shirvan, Development of Cr cold spray-coated fuel cladding with enhanced accident tolerance, Nucl. Eng. Technol. 50 (2018) 229–236, https://doi.org/10.1016/j.net.2017.12.011.

[15] A.S. Kuprin, V.A. Belous, V.N. Voyevodin, V.V. Bryk, R.L. Vasilenko, V.D. Ovcharenko, E.N. Reshetnyak, G.N. Tolmachova, P.N. V'yugov, Vacuum-arc chromium-based coatings for protection of zirconium alloys from the high-temperature oxidation in air, J. Nucl. Mater. 465 (2015) 400–406, https://doi.org/10.1016/j.jnucmat.2015.06.016.

[16] H. Yeom, B. Maier, G. Johnson, T. Dabney, M. Lenling, K. Sridharan, High temperature oxidation and microstructural evolution of cold spray chromium coatings on Zircaloy-4 in steam environments, J. Nucl. Mater. 526 (2019) 151737, , https://doi.org/10.1016/j.jnucmat.2019.151737.

[17] Q.S. Chen, C.H. Liu, R.Q. Zhang, H.Y. Yang, T.G. Wei, et al., Microstructure and high-temperature steam oxidation properties of thick Cr coatings prepared by magnetron sputtering for accident tolerant fuel claddings: the role of bias in the deposition process, Corros. Sci. 162 (2020) 108378, , https://doi.org/10.1016/j.corsci.2019.108378.

[18] G. Bräuer, B. Szyszka, M. Vergöhl, R. Bandorf, Magnetron sputtering – milestones of 30 years, Vacuum 84 (2010) 1354–1359, https://doi.org/10.1016/j.vacuum.2009.12.014.

[19] M. Zaidabadi, G.R. Ansarifar, M.H. Esteki, Thermal hydraulic analysis of VVER-1000 nuclear reactor with dual-cooled annular fuel using K–ω SST Turbulence model, Ann. Nucl. Energy 101 (2017) 118–127, https://doi.org/10.1016/j.anucene.2016.09.027.

[20] D.V. Sidelev, G.A. Bleykher, V.P. Krivobokov, Z. Koishybayeva, High-rate magnetron sputtering with hot target, Surf. Coat. Technol. 308 (2016) 168–173, https://doi.org/10.1016/j.surfcoat.2016.06.096.

[21] A.V. Tumarkin, A.V. Kaziev, D.V. Kolodko, A.A. Pisarev, M.M. Kharkov, G.V. Khodachenko, Deposition of copper coatings in a magnetron with liquid target, Phys. Atom. Nucl. 78 (2015) 1674–1676, https://doi.org/10.1134/S1063778815140136.

[22] J. Vlcek, B. Zustin, J. Rezek, K. Burcalova, J. Tesar, Pulsed magnetron sputtering of metallic films using a hot target, 52nd Annual Technical Conference Proceedings of the Society of Vacuum Coaters, Santa Clara, 2009, pp. 219–223.

[23] J. Musil, M. Jaroš, R. Čerstvý, S. Haviar, Evolution of microstructure and macrostress in sputtered hard Ti(Al,V)N films with increasing energy delivered during their growth by bombarding ions, J. Vac. Sci. Technol. A 35 (2017) 020601, , https://doi.org/10.1116/1.4967935.

[24] J. Musil, Flexible hard nanocomposite coatings, RSC Adv. 5 (2015) 60482–60495.

[25] D.V. Sidelev, G.A. Bleykher, M. Bestetti, V.P. Krivobokov, A. Vicenzo, S. Franz, M.F. Brunella, A comparative study on the properties of chromium coatings deposited by magnetron sputtering with hot and cooled target, Vacuum 143 (2017) 479–485, https://doi.org/10.1016/j.vacuum.2017.03.020.

[26] H. Kersten, H. Deutsch, H. Steffen, G.M.W. Kroesen, R. Hippler, The energy balance at substrate surfaces during plasma processing, Vacuum 63 (2001) 385–431, https://doi.org/10.1016/S0042-207X(01)00350-5.

[27] D.V. Sidelev, E.B. Kashkarov, M.S. Syrtanov, V.P. Krivobokov, Nickel-chromium (Ni–Cr) coatings deposited by magnetron sputtering for accident tolerant nuclear fuel claddings, Surf. Coat. Technol. 369 (2019) 69–78, https://doi.org/10.1016/j.surfcoat.2019.04.057.

[28] I. Efeoglu, R.D. Arnell, S.F. Tinston, D.G. Teer, The mechanical and tribological properties of titanium aluminum nitride coatings formed in a four magnetron closed-field sputtering system, Surf. Coat. Technol. 57 (1993) 117–121, https://doi.org/10.1016/0257-8972(93)90027-L.

[29] D.A. Golosov, Balanced magnetic field in magnetron sputtering systems, Vacuum 139 (2017) 109–116, https://doi.org/10.1016/j.vacuum.2017.02.018.

[30] J.A. Thornton, Influence of apparatus geometry and deposition conditions on the structure and topography of thick sputtered coatings, J. Vac. Sci. Technol. 11 (1974) 666–670, https://doi.org/10.1116/1.1312732.

[31] A. Anders, A structure zone diagram including plasma-based deposition and ion etching, Thin Solid Films 518 (2010) 4087–4090, https://doi.org/10.1016/j.tsf.2009.10.145.

[32] J.V. Cathcart, R.E. Pawel, R.A. McKee, R.E. Druscel, G.J. Yurek, J.J. Cambell, S.H. Jury, Zirconium Metal-Water Oxidation Kinetics IV. Reaction Rate Studies, ORNL/NUREG-17, Aug. (1977).

[33] M.L. Saux, J.C. Brachet, V. Vandenberghe, E. Rouesne, S. Urvoy, A. Ambard, R. Chosson, Effect of a pre-oxide on the high temperature steam oxidation of Zircaloy-4 and M5Framatome alloys, J. Nucl. Mater. 518 (2019) 386–399, https://doi.org/10.1016/j.jnucmat.2019.03.023.

[34] J.G. Gigax, M. Kennas, H. Kim, B.R. Maier, H. Yeom, G.O. Johnson, K. Sridharan, L. Shao, Interface reactions and mechanical properties of FeCrAl-coated Zircaloy-4, J. Nucl. Mater. 519 (2019) 57–63, https://doi.org/10.1016/j.jnucmat.2019.03.004.

[35] X. Han, J. Xue, S. Peng, H. Zhang, An interesting oxidation phenomenon of Cr coatings on Zry-4 substrates in high temperature steam environment, Corros. Sci. 156 (2019) 117–124, https://doi.org/10.1016/j.corsci.2019.05.017.

[36] K. Taneichi, T. Narushima, Y. Iguchi, C. Ouchi, Oxidation or nitridation behavior of pure chromium and chromium alloys containing 10 mass% Ni or Fe in atmospheric heating, Mater. Trans. 47 (2006) 2540–2546, https://doi.org/10.2320/matertrans.47.2540.

[37] E.A. Gulbransen, K.F. Andrew, A preliminary study of the oxidation and vapor pressure of chromium, J. Electrochem. Soc. 99 (1952) 402.

[38] P. Kofstad, K.P. Lillerud, On high temperature oxidation of chromium: II. Properties of Cr_2O_3 and the oxidation mechanism of chromium, J. Electrochem. Soc. 127 (1980) 2410–2419.

[39] C. Meng, L. Yang, Y. Wu, J. Tan, W. Dang, X. He, X. Ma, Study of the oxidation behavior of CrN coating on Zr alloy in air, J. Nucl. Mater. 515 (2019) 354–369, https://doi.org/10.1016/j.jnucmat.2019.01.006.

[40] D.J. Young, High Temperature Oxidation and Corrosion of Metals / Oxford, Elsevier, UK, 2008 – 573 pp.

[41] R.A. Perez, H. Nakajima, F. Dyment, Diffusion in -Ti and Zr, Mater. Trans. 44 (2003) 2–13, https://doi.org/10.2320/matertrans.44.2.

Repository KITopen